Proceedings of IMECE'04
2004 ASME International Mechanical Engineering Congress & Exposition
Anaheim, California, USA, November 13-19, 2004

IMECE2004-61752

FLOW AND HEAT TRANSFER OF MICROFOAMS IN HORIZONTAL MINICHANNELS

Howard Tseng
Laurent Pilon

University of California, Los Angeles
Mechanical and Aerospace Engineering
420 Westwood Plaza
Los Angeles, CA 90095-1597
pilon@seas.ucla.edu

ABSTRACT

Colloidal gas aphrons (CGA) consists of closely packed minute gas bubbles with diameter ranging from 10 to 100 microns. It is produced by stirring a surfactant solution at high speed in a fully baffled beaker. CGA can be used in various applications such as bioremediation, bioreactors, oil recovery, and fire fighting. This paper reports experimental data for (1) adiabatic flow and (2) convective heat transfer of CGA into five 1.58 x 0.76 mm^2 mini-rectangular channels. First, it is shown that CGA is a shear thinning fluid. Correlation for the Fanning friction factor as a function of Reynolds number is compared with that of water and *macro*foams. Then, the local temperature and heat transfer coefficient along the mini-channels are reported as a function of the mass flow rates and imposed heat flux. The heat transfer coefficients for CGA appears to be constant and independent of mass flow rate and imposed heat flux as well known in the case of single phase laminar flow.

INTRODUCTION

Colloidal Gas Aphrons (CGA), also called microfoams, consist of bubbles between 10 and 100 µm in diameter with a porosity of up to 70%. They can be produced by stirring an aqueous surfactant solution contained in a fully baffled beaker at room temperature, as described in Figure 1 [1]. The solution is stirred by a spinning disk driven at 5,000 to 10,000 rpm by an electrical motor. Two to four baffles are equally spaced around the container and extend well above the surface of the solution. Once a critical stirring speed has been reached, waves are produced at the liquid surface. The waves beat up against the baffles and are forced to re-enter the liquid at the baffles. It is believed that the re-entering liquid carries a thin film of gas which becomes sandwiched between the liquid and the baffle. Such a thin film is unstable and breaks into microscopic bubbles encapsulated by a soapy shell, i.e. minute gas aphrons. After a few minutes of stirring, CGA forms and rises at the surface of the solution. It has been reported that CGAs made of water and surfactant solutions (i) have stable bubbles with a narrow and reproducible size distribution between 10 and 100 µm (see Figure 2), (ii) exhibit high stability, (iii) separate easily from the bulk liquid phase, and (iv) can be easily pumped through tubes while keeping their structure [1]. However, even though the flow properties of CGA have been discussed qualitatively in the literature, to the best of our knowledge, no quantitative data on the rheology, pressure drop, and Fanning friction factor associated with CGA flow rates has been reported.

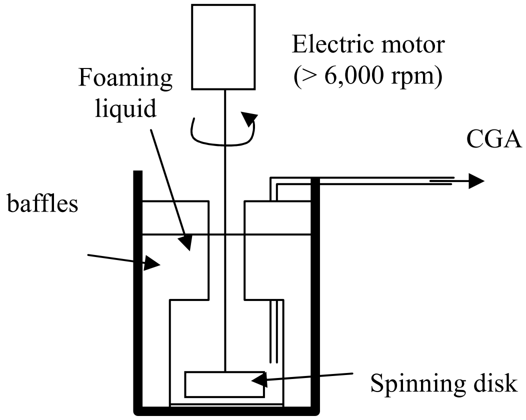

Figure 1. Schematic of the CGA forming process

Colloidal gas aphrons are subject to the same physical phenomena as those taking place in foams including (i) liquid drainage, (ii) interbubble gas diffusion, and (iii) Gibbs-Marangoni effects. However, capillary drainage or Plateau border suction effect occurring in polyhedral foams [2] does not take place in CGA as bubbles are spherical (Figure 2). Moreover, buoyancy caused by the density difference between the gas and the liquid phases is relatively limited due to the small size of the microbubbles that act as colloidal particles.

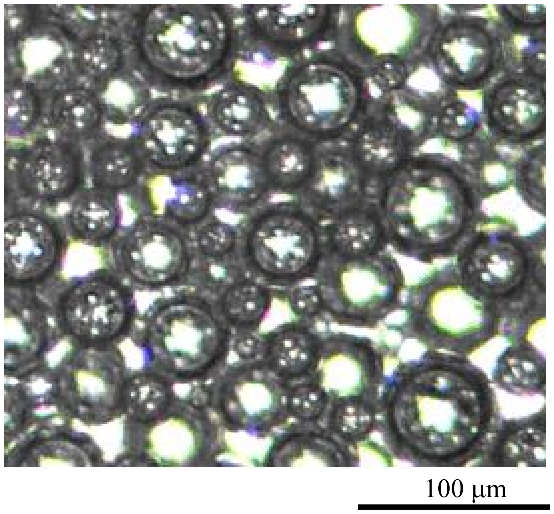

Figure 2. Micrograph of closely packed CGA bubbles

Most applications of colloidal gas aphrons take advantage of (i) their large interfacial area, (ii) the adsorption of particles at the microbubble interfaces, and (iii) their stability for enhanced mass transfer [3]. Applications include

Separation

Application of CGAs to separation technology include (i) remediation of soils contaminated with hydrocarbons [4,5], (ii) cleaning of water contaminated with metals [6,7] or organic dyes [8,9], (iii) protein separation [10-12] in replacement of a combination of processes including centrifugation, filtration, extraction and chromatography, (iv) cell flotation [13] such as yeast-cells [14], (iv) mineral extraction by flotation [15], (v) algae removal from contaminated waters [1].

Oil Recovery

CGA have been used for clean of sand contaminated with oil [5] and could be used for oil recovery when foams are currently being used. Experiments shows that CGA formed with anionic surfactants percolate through sand carrying most of the oil [1]. Note that CGA formed with cationic surfactant will not percolate through the sand bed [1].

Firefighting

Foam is currently used for fire fighting by covering the burning material with a thick layer of foam. However, it is not easy to pump large flow rates of foams through often long pipes and various fittings [16]. Moreover, pipe fitting are responsible for pressure drop much larger in foam flows than in single phase water flows [16]. Colloidal gas aphrons were reported "to flow like water" [1] and therefore could be used for fire fighting as they can travel longer distances than foam for identical pumping power or pressure drop. Thus, they could increase mobility, reactivity, and safety of fire-fighters. Sebba [1] also indicated that CGA made of a surfactant mixture can very effectively extinguish gasoline fire. A mixture of anionic and cationic surfactant was shown to spread over the gasoline and extinguish the fire.

Fermentation and Bioreactors

Applications of CGA to fermentation take advantage of their large interfacial area and their long lifetime and slow rise. Indeed, fermentation reactors based on bubble columns or bioreactors are often mass transfer limited due to (1) relatively small interfacial area and (2) rapid rise and thus short residence time of the large bubbles through the reactor. The use of CGA was instrumental in increasing oxygen transfer from the bubble to the solution and resulted in faster growth of oxygen consuming micro-organisms [1].

In most of these applications, CGA is pumped through pipes and fitting under different temperatures. For this reason, it is necessary to understand the rheology and the heat transfer properties of CGA.

NOMENCLATURE

A_t	Overall area of the channels, m^2
c_p	specific heat, J/kgK
D_h	hydraulic diameter, mm
G	mass flux, kg/m^2s
h	local heat transfer coefficient, W/m^2K
$\overline{h}$	average heat transfer coefficient, W/m^2K
H	Channel height, m
I	Current, A
k	thermal conductivity, W/mK
L	channel length, m
$\dot{m}$	total mass flow rate, kg/s
M_{CGA}	Mass of CGA, kg
P	channel perimeter, m
ΔP	overall pressure drop, Pa
Q_f	total volumetric flow rate, m^3/s
q	heat transfer rate, W
q"	heat flux, W/m^2
T	Temperature, K
u	average fluid velocity, m/s
V	Power supply voltage, V
V_{CGA}	Volume of CGA, m^3
W	Channel width, m
f	Fanning friction factor
Re	Reynolds number
Nu	Nusselt number
$\dot{\gamma}_w$	effective shear rate, 1/s
$\dot{\gamma}_a$	apparent shear rate, 1/s
μ_e	effective dynamic viscosity, mPa.s
ρ	density, kg/m^3
τ_w	wall shear stress, Pa

EXPERIMENTAL SETUP

Figure 3 shows a schematic of the cross-section of the test section. The design is similar to that used by Warrier *et al.* [17] to study boiling heat transfer in mini-channels. Five identical rectangular parallel mini-channels have been machine etched into Lexan® polycarbonate top. They are mated with an aluminum bottom plate. An Iconel-625 strip is placed beneath the aluminum plate and has the same dimensions of 6.35 mm wide and 30.72 cm long. An additional Teflon® strip of identical dimension is placed under the heating element to assure good thermal contact with the aluminum plate and provide electrical insulation. A Sorensen DC S60-20E power supply with voltage ranging from 0 to 60 volts and current ranging from 0 to 125 A is used for resistance heating of the Iconel-625 strip. Each flow channel has a hydraulic diameter D_h of 1.03 mm. The total length to diameter ratio is 433.5, while the effective heated length to diameter ratio is 409.8. The distance between the centers of any two adjacent channels is 3.0 mm. The apparatus rests on a G10 board with slots cut into the board. Two Omega PX26-015DV pressure transducers are used to measure the overall pressure drop between the inlet and the outlet of the channels. The inlet and outlet temperatures are measured by type K thermocouples. Moreover, to measure the surface temperature along the aluminum plate, ten indentations were made in the aluminum plate. Holes were machined into the Teflon® and Inconel-625 strips to allow the thermocouples to pass through. They allow ten type-K thermocouples to be secured on the aluminum by high thermal conductivity thermocouple cement. There are two thermocouples per axial location and the temperature readings at each axial location did not differ by more than ±0.2°C for all heat transfer experiment. The average of both temperatures is taken as the temperature of the heated surface at that axial location. The large thermal conductivity of the aluminum plate allows for uniform heat flux along the channels. Also, the temperature of the aluminum plate at a given cross-section perpendicular to the flow is assumed to be uniform by virtue of the fact that the Biot number ($Bi=h/k_{Al}$) is much smaller than 1. Thus, the surface temperature in the channel is identical to that measured at the aluminum plate/heating strip interface. Also, heat losses through the Lexan® top are neglected due to its low thermal conductivity (0.2 W/mK). They were conservatively estimated to be 1 W or less than 3% of the total heat input.

As mentioned by Warrier *et al.* [17], it was not possible to measure the fluid flow temperature inside the channels because the thermocouples were in contact with the channel walls leading to a higher temperature reading. Instead, the local fluid temperature is computed using the local energy balance equation. All thermocouples are calibrated by flowing liquid water of a known temperature adiabatically through the test apparatus. To minimize contact resistance between the Iconel-625 heating strip and the aluminum bottom plate, several clamps are used to ensure good thermal contact between the heating strip and the aluminum plate. All the thermocouples and pressure readings are recorded every second by an IOTECH DAQTEMP 14A data acquisition system connected to a PC computer.

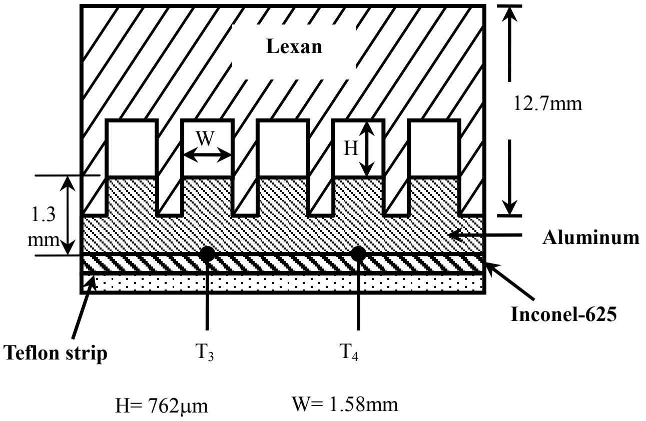

Figure 3. Cross-section of the mini-channels

Experimental Procedure

Figure 4 shows the water experimental setup, which consists of (i) a fifteen gallon Nalgene supply tank, (ii) a Cole-Parmer model 75225 volumetric pump, (iii) a Cole-Parmer P-32464-46 single float flowmeter (rotameter type), (iv) the test section, (v) Sorensen DC S60-20E power supply, and (vi) the return tank.

For the water experiments, the same methodology as described in Warrier *et al.* [17] is followed. First, the liquid is preheated in the supply tank. After reaching the desired temperature, it is pumped through the flowmeter into the test section where a heat flux may be applied. Each experiment is allowed to run for a minimum of 10 minutes so that steady state conditions are reached. Then, the data acquisition unit is turned on to record the pressures and temperatures. The typical overall duration of a single experiment is about 20 to 25 minutes.

For adiabatic tests, the power to the heating element is turned off and the temperature along the length of the channels is constant. Water then flows out of the test section and into the return tank, where it is cooled off by chilled water running through copper tubes. When the water has reached 23°C, it is then drained back into the supply tank. This process is repeated for each water experiment.

For convective heat transfer experiments, the volumetric flow rate of water is first fixed to a particular rate. Then, the current and voltage settings are fixed. When the experiment is completed, the current and voltage are changed for the same flowrate. The process is repeated for different flow rates.

For the CGA experiments, the experimental setup is similar to that used with water except that the supply tank is replaced by a fully baffled container as shown in Figure 1. The flowmeter is also removed as it strongly affects the CGA morphology. Instead, the mass and volumetric flow rates are determined by measuring the mass $M_{CGA}(t)$ and the volume $V_{CGA}(t)$ of the CGA flowing in and out of the test section as a function of time. Moreover, since the mass of air is significantly smaller than that of water, we assume that $M_{total}(t) \approx M_{water}(t)$. Then, the porosity of CGA can be expressed as

$$\phi(t) = \frac{V_{gas}}{V_{CGA}(t)} = 1 - \frac{M_{CGA}(t)}{\rho_{water} V_{CGA}(t)} \qquad (1)$$

It was found to be independent of flow rate and heat flux and equal to 0.7 ± 0.03.

Finally, samples of CGA was taken at the inlet and outlet of the test section and observed under a Leica DM IL microscope (Figure 2). it was verified that both the porosity and the bubble size distribution remains unchanged as CGA travels through the mini-channels. It was noticed that for convective heat transfer experiments the porosity and bubble diameter tend to increase slightly due to gas expansion but within the experimental uncertainty.

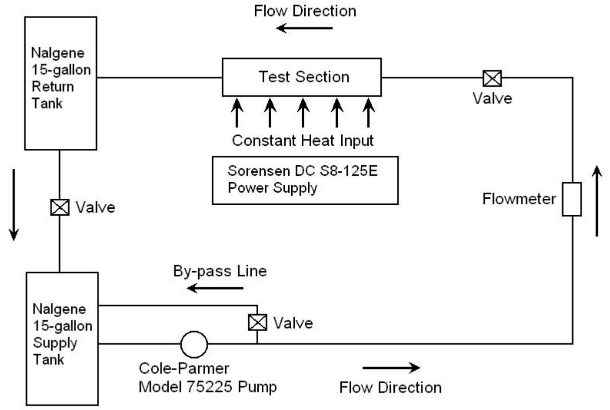

Figure 4. Water flow loop

According to the specifications of the Omega PX26-015DV pressure transducers, there is a 1% error reading on the pressure reading corresponding to an absolute error of 1000 Pa. The tubing connecting the pressure transducers to the inlet and outlet fixtures was filled with water to reduce the error readings on the pressure.

The thermocouples have been calibrated by flowing water through the test section under adiabatic conditions at temperature ranging from 25 to 50^{o}C. The mean difference between each of the thermocouples and the fluid temperature was ±0.2°C. Steps are also taken to try to minimize the influence of the heating element on the thermocouple wire by enlarging thermocouple passages in the Inconel-625 strip.

For water experiments, the volumetric flow rate is measured directly with the Gilmont flowmeter as described in the experimental setup section. The flowmeter is first calibrated by setting it to a particular setting and then letting the water be pumped into a graduated cylinder. A stop watch is used to measure the time it takes to fill a certain volume. The error in the measurement is the error on the graduated cylinder, which is described at ±5% of the marked reading at 25°C. For CGA, the same graduated cylinder is also used to measure the volumetric flow rate.

The mass flow rates for the water experiments are calculated by multiplying the density of water [18] by the volumetric flow rate. The error associated with the water mass flow rates is the same as the error of the graduated cylinder used for the calibration of the flowmeter. For CGA, the mass was measured at different times using a scale with an error reading of ±1 gram. The mass flow rate were computed by curve fitting the plot of mass versus time over a period of time larger than 300s with a correlation coefficient. It varied from 0.9 to 9 g/s.

RHEOLOGY OF COLLOIDAL GAS APHRONS

Effective dynamic viscosity

Colloidal gas aphrons is treated as a pseudo-homogeneous time-independent non-Newtonian fluid obeying power-law behavior in steady-state laminar flow and having effective dynamic viscosity μ_e. The wall shear stress τ_w, shear rate $\dot{\gamma}_w$, and the apparent shear rate are related by

$$\tau_w = k\dot{\gamma}_w^n = \mu_e \dot{\gamma}_a \qquad (2)$$

where k and n are the flow consistency and flow behavior, respectively. If n = 1, then the fluid is Newtonian and k its viscosity. Moreover, the wall shear rate is defined in terms of the apparent shear rate by the Rabinowitsch-Mooney relationship expressed as

$$\dot{\gamma}_w = \left(\frac{3n+1}{4n}\right)\dot{\gamma}_a \qquad (3)$$

The wall shear stress τ_w and the apparent shear rate $\dot{\gamma}_a$ are experimentally determined from the pressure drop ΔP and the volumetric flow rate Q_f per channel as [16],

$$\tau_w = \frac{D_h \Delta P}{4L} \quad \text{and} \quad \dot{\gamma}_a = \frac{8u_f}{D_h} \qquad (4)$$

Figure 5 shows the shear stress and the viscosity of single phase water and CGA as a function of the apparent shear rate under adiabatic conditions at 24°C for CGA and 35°C for water. First, the validity of the experimental procedure and data analysis procedures is demonstrated by the single phase water data. Indeed, water data indicates that the shear stress is linearly proportional to the shear rate, i.e., water is a Newtonian fluid with a viscosity of 0.67 mPa.s at 35^{o}C. This value falls within 8% of the tabulated value of 0.725 mPa.s [18].

On the other hand, CGA behaves as a shear thinning fluid for which the effective dynamic viscosity decreases with apparent shear rate. The shear stress and shear rate correlate as follows

$$\tau_w = 0.115\dot{\gamma}_a^{0.53} \qquad (5)$$

corresponding to an effective dynamic viscosity of

$$\mu_e = 0.115\dot{\gamma}_a^{-0.47} \qquad (6)$$

The above correlations for the shear stress and effective dynamic viscosity as a function of shear rate have regression coefficients of 0.91 and 0.88, respectively.

Moreover, rheology experiments with a TA Instrument AR 2000 rheometer equipped with a 2°- 60 mm shearing cone have been performed in the shear rates range from 1 to 500/s. However, the morphology of CGA changes rapidly and no steady-state could be reached.

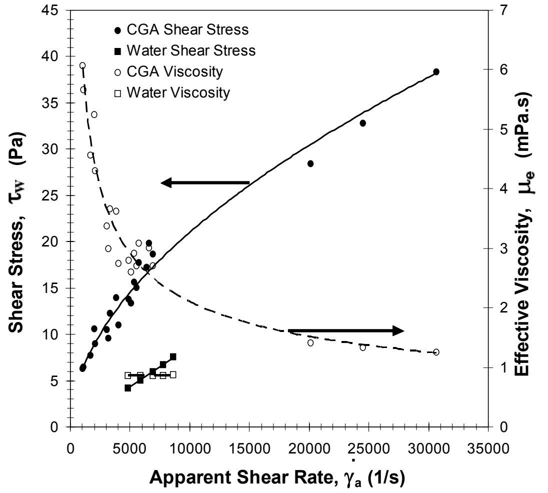

Figure 5. Shear stress and effective dynamic viscosity versus apparent shear rate for both water and CGA at 25 °C.

Fanning friction factor vs. Reynolds Number

The Fanning friction factor is defined as [18]

$$f = \frac{\tau_w}{\rho u^2 / 2} \tag{7}$$

where τ_w is the wall shear stress and ρ is the fluid density. The average fluid velocity u in a single channel is calculated by dividing the volumetric flow rate by the overall cross sectional area of the channels, i.e., $u=Q_f/5WH$. The Fanning friction factor for single phase water in laminar flow in a rectangular channel of cross section (1.58x0.76 mm^2) is given by [18]

$$f_{1\phi} = \frac{15.5}{Re} \tag{8}$$

where Re is the Reynolds number, defined as

$$Re = \frac{GD_h}{\mu} \tag{9}$$

where G is the mass flux and μ is the fluid viscosity. Similarly, the Fanning friction factor for foam flowing in cylindrical pipe has been reported as [16]

$$f_{foam} = \frac{15.97}{Re^{0.99}} \tag{10}$$

where the Reynolds number is computed from the effective foam viscosity [16]. To the best of our knowledge, no Fanning friction factor has been reported for CGA flow. However, it is essential in designing and scaling up bench-top experiments to industrial processes and in predicting pressure drop and pumping power.

The Fanning friction factor for CGA can be calculated using Equation (7). The density of the CGA is experimentally determined by dividing the measured mass flow rate by the volumetric flow rate. The Reynolds number for CGA is defined based on the effective dynamic viscosity μ_e of the CGA defined by Equation (6). Figure 6 shows the plot of the Fanning friction factor vs. the Reynolds number for both single phase water and CGA in rectangular channels and foam in cylindrical pipes. One can see that the Fanning friction factor for CGA is similar to the correlation derived for single phase flow. However, the effective dynamic viscosity is much higher than that of water.

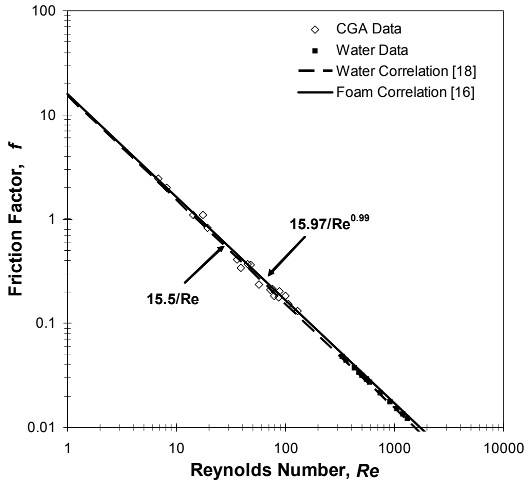

Figure 6. Friction factor versus Reynolds number

CONVECTIVE HEAT TRANSFER

Heat Loss

To determine the heat loss of the power supply to the surrounding environment, an energy balance is performed on the heated water. The total power input is expressed by Joule's law,

$$q_{total} = VI \tag{11}$$

where V is the voltage measured in volts and I is the current measured in ampere. The actual heat input into the test section $q_{channels}$ must account for the heat loss to the surrounding and is given by

$$q_{channels} = q_{total} - q_{loss} \tag{12}$$

It can also be calculated from the energy balance on the single phase water

$$q_{channels} = \dot{m} c_p (T_{outlet} - T_{inlet}) \tag{13}$$

where $\dot{m}$ is the mass flow rate and c_p is the specific heat of water. Figure 7 plots the $q_{channels}$ computed by Equation (13) and q_{total} measured using Equation (11). From the plot, it can be seen that the actual power input is very similar to the total power input. It was found that the heat loss to the environment q_{loss} varies linearly with the total power input q_{total} and represents 8% of the total heat input over the range from 42 to 130W. In other words, 92% of the total power consumed is supplied to the test section.

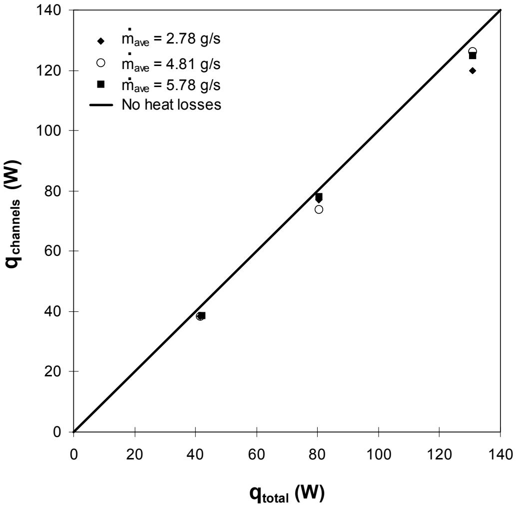

Figure 7. Actual power input into the channels versus total power input for water.

Specific Heat of CGA

The specific heat, $C_{p,CGA}$, for CGA is not known but can be determined using the energy balance equation

$$c_{p,CGA} = \frac{q_{channels}}{\dot{m}(T_{outlet} - T_{inlet})} \tag{14}$$

In the present study, the experimental data indicate that the average specific heat of generated CGA is 3966 J/kgK. The specific heat of CGA can be modeled as a air mass fraction x,

$$c_{p,CGA} = (1-x)c_{p,H_2O} + xc_{p,air} \tag{15}$$

where x is the mass fraction of air on CGA, i.e.,

$$x = \rho_{air}\phi / [\rho_{air}\phi + \rho_{H_2O}(1-\phi)] \tag{16}$$

Then, the predictions of Equation (15) fall within 10% of the experimental values. Since the experimental test section and procedure remain the same for both CGA and water, it is assumed that the $q_{channels}$ for CGA represents also 92% of q_{total}.

Local Temperature Profile

As previously mentioned, the local fluid temperature along the channels is not measured. Instead, it is calculated using the energy balance equation

$$T_f(x) = T_{f,in} + \frac{q_{channels}}{\dot{m}c_p}x = T_{f,in} + \frac{T_{f,out} - T_{f,in}}{L}x \tag{18}$$

where $T_{f,,in}$ and $T_{f,,out}$ are the measured fluid inlet and outlet temperatures, $\dot{m}$ is the mass flow rate, and x is the axial location of the thermocouple along the flow channel measured from the channel entrance.

Figures 8 and 9 show the typical wall and fluid temperature profiles along the length of the channel for water and CGA, respectively. In both cases, the mass flow rate is 7.7 × 10^{-4} kg/s and the total heat input in the channels is 36 W. The difference between the fluid and the wall surface temperature increases in the entry region and remains constant in the fully developed region for both water and CGA. However, the temperature difference is much larger for CGA leading to a smaller heat transfer coefficient as discussed later.

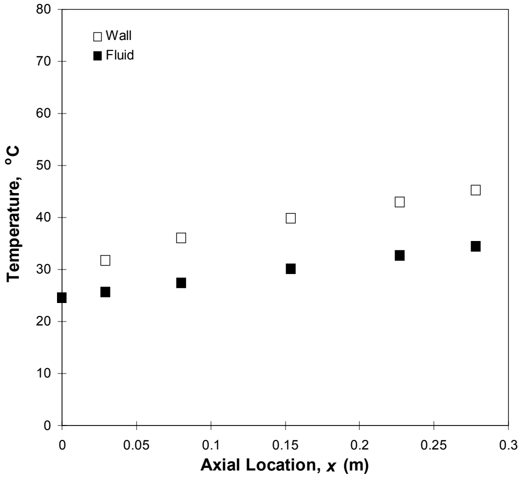

Figure 8: Fluid and wall temperatures for water at total volumetric flow rate of 2.9 × 10^{-6} m^3/s and power input of 130 W.

Nusselt Number and Heat Transfer Coefficient

The local heat transfer coefficient can be calculated according to

$$h(x) = \frac{q''_w}{T_w(x) - T_l(x)} \tag{19}$$

where $T_w(x)$ is the measured wall temperature of at the location of the thermocouple and $T_l(x)$ is the fluid temperature calculated using Equation (18). The wall heat flux q''_w is assumed to be uniform along the aluminum plate thanks to its large thermal conductivity. It is calculated from the overall heat input $q_{channels}$ in the five channels and is given by

$$q''_w = \frac{q_{channels}}{A_t} \tag{17}$$

where A_t is the total surface area of the flow channels. For the five channels, $A_t = 5WL$ where W and L are the width and length of a single channel.

For validation purposes, the single phase water data are presented in terms of the local Nusselt number Nu_x defined as

$$Nu_x = \frac{h(x)D_h}{k_f} \tag{20}$$

where D_h is the hydraulic diameter of the channel and k_f is the fluid thermal conductivity. Kays and Crawford [19] reported numerical simulations of convective heat transfer in rectangular channels with aspect ratio of 2.00 and 2.33. The aspect ratio of the channels under consideration is 2.08 and falls between the two simulated geometries.

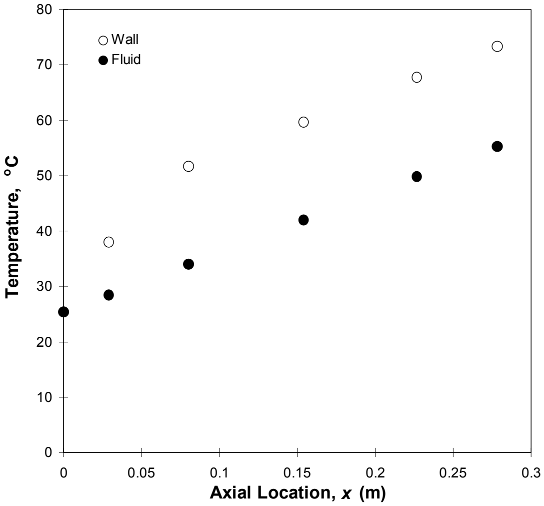

Figure 9: Fluid and wall temperatures for CGA at total volumetric flow rate of 2.9 × 10^{-6} m^3/s and power input of 130 W.

Figure 10 shows the evolution of the local Nusselt number along the axial locations of the channel for single phase water and heat fluxes ranging from 36 to 220W. The Nusselt number decreases in the entry region to reach a constant value nearly independent of heat flux in the fully developed region. Moreover, one can see that the experimental data falls between the simulated values, except at the entry region. These results confirm the accuracy of the instruments and the validity of the data analysis. Therefore, the same analysis method can be applied to CGA. In the case of CGA, the local heat transfer coefficient *h(x)* can be determined using Equation (19). However, the Nusselt number cannot be calculated since the thermal conductivity of CGA is unknown unless one uses possibly unreliable models. Since the conductivity is constant at a given temperature, it was preferred to plot the local heat transfer coefficient versus the axial length of the channels. Figure 11 compares the local heat transfer coefficient *h(x)* versus the axial length of the channels obtained for water and CGA at different heat transfer rates and identical mass flow rates. In both cases, the heat transfer coefficient appears to be nearly independent of the heat input. Moreover, the convective heat transfer rate achieved with CGA is much less than water for the same heat flux and mass flow rate.

Finally, the average heat transfer coefficient is defined as

$$\overline{h} = \frac{1}{A_s}\int h(x)dA_s \tag{21}$$

where A_s is the surface area per channel, i.e., A_s= WL where W is the width and L is the length of the channel. Figure 12 shows the plot of the average heat transfer coefficient versus the mass flow rate. It indicates that the average heat transfer coefficient for both water and CGA is independent of mass flux. The correlation for single-phase laminar flow with constant heat flux is expressed as $Nu = \overline{h}D_h / k_f = 4.19$ [19] and predicts that the average heat transfer coefficient for water is 2552 W/m^2K.

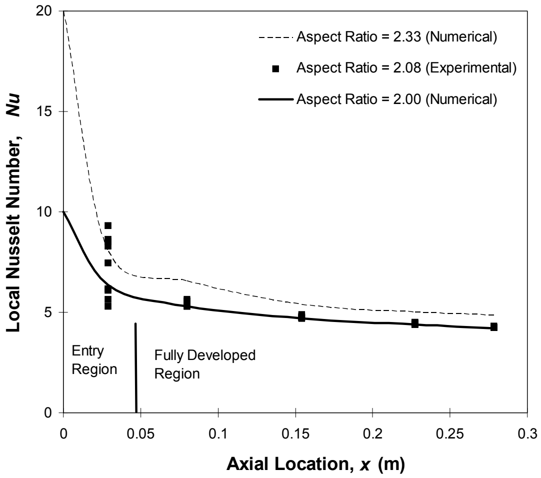

Figure 10. Local Nusselt number along the axial length of the channels for water.

On the other hand, the experimental average heat transfer coefficient for water was found to be 3057 W/m^2K (Nu=5.0) and fall within 16% of the correlation value stated above. For CGA it is reduced by 46% compared to water at 1660 W/m^2K. This can be attributed to the large porosity of CGA resulting in significant reduction in specific heat. Finally, note that for both water and CGA, the Biot number for the aluminum plate is less than 0.02 confirming our initial approximation.

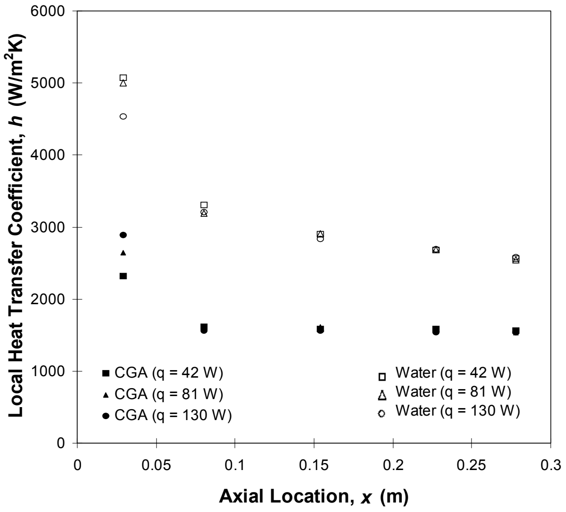

Figure 11. Local heat transfer coefficient along the axial length of the channels for both water and CGA

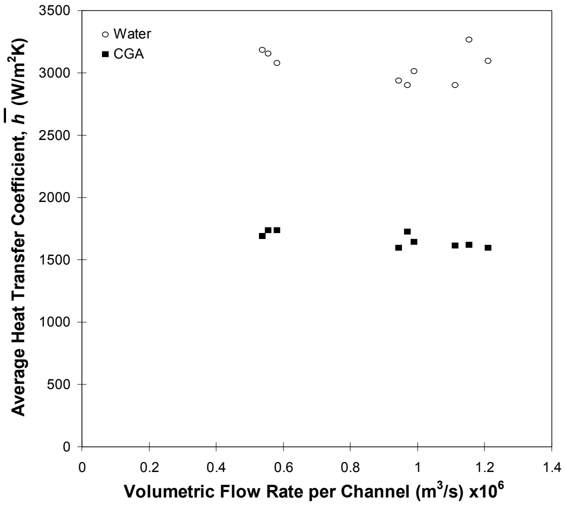

Figure 12. Average heat transfer coefficient versus the mass flux in the channels for both water and CGA.

CONCLUSION

The present study has been concerned with rheology and heat transfer properties of colloidal gas aphrons flowing in rectangular mini-channels of hydraulic diameter 1.03 mm (1.58cm x 762µm). The following conclusions can be drawn:

1. CGA behaves as a shear thinning fluid.
2. The Fanning friction factor for CGA in laminar flow follows the same law as single phase.
3. the local and average heat transfer coefficients for CGA under imposed heat flux and laminar flow conditions are independent of mass flow rate and heat flux. They are smaller than those for water due to the high porosity of the CGA resulting in low specific heat and thermal conductivity.

ACKNOWLEDGMENTS

The authors would like to thank Dr. G. Warrier and Prof. V. Dhir for useful technical discussions and assistance in performing the experiments.

REFERENCES

[1] Sebba, F., 1987, *Foams and Biliquid Foams-Aphrons*, John Wiley & Sons, New York.

[2] Bhakta A and Ruckenstein E., 1997, “Decay of standing foams: drainage, coalescence and collapse”, Advances in Colloid and Interface Science, **70**, pp. 1-124.

[3] Bredwell M.D. and Worden R.M., 1998, “Mass transfer properties of microbubbles: 1) Experimental studies”, Biotechnology Progress, **14**, pp. 31-38.

[4] Kommalapati R.R., Valsaraj K.T., Constant W.D. and Roy D., 1998, “Soil flushing using colloidal gas aphron suspensions generated from a plant-based surfactant”, Journal of Hazardous Materials, **60**, pp. 73-78.

[5] Roy D., Valsaraj K.T., Constant W.D. and Darji M., 1994, “Removal of hazardous oily waste from a soil matrix using surfactants and colloidal gas aphron suspensions under different flow conditions”, Journal of Hazardous Materials, **38**, pp. 127-144.

[6] Ciriello S., Barnett S.M. and Deluise F.J., 1982, “Removal of heavy-metals from aqueous-solutions using microgas dispersions, Separation Science and Technology”, **4**, pp. 521-534.

[7] Cabezon L., Caballero M., Diaz J., & Perezbustamante J.A., 1991, “Multi-elemental separation and determination of some heavy-metals (Cu, Co, Cd, and Ni) in tap water and high salinity media by CGA (Colloidal Gas Aphron) coflotation”, Analysis, **4**, pp. 123-127.

[8] Roy D., Valsaraj K.T. and Kottaisa SA., 1992, “Separation of organic-dyes from waste-water by using colloidal gas aphrons”, Separation Science and Technology, **27**, pp. 573-588.

[9] Basu S. and Malpani P.R., 2001, “Removal of methyl orange and methylene blue dye from water using colloidal gas aphron-effect of processes parameters”, Separation Science and Technology, **13**, pp. 2997-3013.

[10] Noble M., Jauregi P., Kaul A. and Varley J., 1998, “Protein recovery using gas-liquid dispersions”, Journal of Chromatography, **1-2**, pp. 31-43

[11] Jauregi P., Varley J. and Gilmour S., 1997, “Characterization of colloidal gas aphrons for subsequent use for protein recovery”, Chemical Engineering Journal, (**65**), pp. 1-11.

[12] Jauregi P. and Varley J., 1998, “Colloidal gas aphrons: A novel approach to protein recoveryy”, Biotechnology and Bioengineering, **59**, pp. 471-481.

[13] Subramaniam M.B., Blakebrough N., Hashim M.A., 1990, “Clarification of suspensions by colloidal gas aphrons”, Journal of Chemical Technology and Biotechnology, **48**, pp. 41-60.

[14] Hashim M.A., Sengupta B., and Subramaniam M.B., 1995, “Investigations of the flotation of yeast-cells by colloidal gas aphrons (CGA) dispersions”, Bioseparation, **5**, pp. 167-173.

[15] Cilliers J. J. and Bradshaw D. , 1996, “The flotation of fine pyrite using colloidal gas aphrons”, Minerals Engineering, **9**, pp. 235-241.

[16] Deshpande N.S. and Barigou M., 2001, “The flow of gas-liquid foams through pipe fittings”, International Journal of Heat and Fluid Flow, **22**, pp. 94-101.

[17] Warrier G.R., Dhir V.K. and Momda L.A., 2002, “Heat transfer and pressure drop in narrow rectangular channels”, Experimental Thermal and Fluid Sciences, **26**, pp. 53-64.

[18] Munson, B.R., Young, D.F. and Okiishi, T.H., 1994, *Fundamental of Fluid Mechanics*, John Wiley & Sons, New York.

[19] Kays, W.M and Crawford, M.E., 1983, *Convective Heat and Mass Transfer*, McGraw-Hill, New York.